Available online at www.sciencedirect.com
SCIENCE DIRECT®
Nuclear Instruments and Methods in Physics Research A 501 (2003) 119–125
NUCLEAR INSTRUMENTS & METHODS IN PHYSICS RESEARCH Section A
www.elsevier.com/locate/nima

# The ALICE Silicon Drift Detector system

D. Nouais[a,*], S. Beolè[a], M. Bondila[b,1], V. Bonvicini[c], P. Cerello[a], E. Crescio[a], P. Giubellino[a], M. Idzik[a], A. Kolozhvari[a,b], S. Kouchpil[d], E. Lopez Torres[a], M.I. Martinez[a,e], G. Mazza[a], S. Piano[c], C. Piemonte[c], A. Rashevsky[c], L. Riccati[a], A. Rivetti[a], F. Tosello[a], W.H. Trzaska[b], A. Vacchi[c], R. Wheadon[a]

[a] *INFN, Sezione di Torino, Via P. Giuria 1, Torino 10125, Italy*
[b] *Jyväskylä University, Finland*
[c] *INFN, Sezione di Trieste, Italy*
[d] *ŘEž, Czech Republic*
[e] *CINVESTAV, Mexico City, Mexico*

For the ALICE Collaboration

**Abstract**

The project of the two Silicon Drift Detector (SDD) layers of the ALICE Inner Tracking System is reviewed, with details on the barrel construction and on the front-end electronics. The results on the SDD spatial resolution are reported as obtained in the 2000 beam test from a whole drift region of the detector.


*PACS:* 29.40.W; 29.40.G; 85.40; 61.72.T

*Keywords:* Silicon detectors; Drift detectors; Position sensitive detectors; Tracking

## 1. Introduction

The central detector of ALICE [1,2] will consist of an Inner Tracking System (ITS) [3,4] whose basic functions are the secondary vertex reconstruction of hyperon and charm decays, the particle identification and the tracking of low-momentum particles, and the improvement of the overall momentum resolution. The system, which covers the polar angular range $90 \pm 45$ deg. over the full azimuth, is embedded in a large solenoidal magnet generating a field between 0.2 and 0.5 T. According to the highest theoretical estimation, the number of charge particles per unit of pseudo-rapidity in central Pb + Pb collision is expected to be 8000 at $\eta = 0$.

Because of this high particle density, the innermost four layers need to be truly two-dimensional devices. To give the inner tracking system a stand-alone particle identification capability, a minimum of four layers need an analogue readout with a wide enough dynamic range to provide unsaturated $dE/dx$ measurements down to the minimum momentum ($P_t = 50$ Mev/$c$) for which the tracks

*Corresponding author. Fax: +39-11-6699579.
*E-mail address:* nouais@to.infn.it (D. Nouais).
[1] Also at Institute of Space Sciences, Bucharest.

0168-9002/03/$ - see front matter 
doi:10.1016/S0168-9002(02)02020-X

have a reasonable (> 20%) reconstruction probability. To achieve this performance, the ITS will consist of six barrels of high-resolution silicon tracking detectors:

- two layers of Silicon Pixel Detectors (SPDs) with digital readout,
- two layers of Silicon Drift Detectors (SDDs) with analogue readout,
- two layers of double-sided silicon micro-strip detectors (SSDs) with analogue readout.

Silicon Drift Detectors have been chosen to equip the third and the fourth layers of the ITS due to their characteristics: very high-resolution two dimensional sensors suitable for high track-density experiments. The charge particle density is expected to be 7.2 $cm^{-2}$ on the inner SDDs layers (radius 15 cm) and 2.7 $cm^{-2}$ on the outer one (radius 24 cm). The maximum usable luminosity is limited by the event pile-up probability in the Time Projection Chamber [2], whose drift time is about 90 μs. Assuming a hadronic interaction cross-section of 8 b for Pb–Pb collision, and a luminosity of $10^{27}$ $cm^{-2}$ $s^{-1}$, the pile-up probability amounts to 7.7% in the SDD. In an SDD, the electrons released during the passage of a particle drift under the effect of an applied electric field along a direction parallel to the surface of the wafer toward an array of collecting anodes. The drift velocity is proportional to the electric field $E$ and to the electron mobility $\mu_e$: $v = \mu_e E$. In this way, the distance of the crossing point from the anodes is determined by the measurement of the drift time. The second coordinate is obtained from the centroid of the charge distribution across the anodes. As a consequence of this principle, the number of front-end channels necessary to read out large area detectors is very small compared to other detectors with comparable spatial resolution. The reduced number of electronic channels allows the front-end to provide the energy loss measurement without increasing too much the power budget.

In Section 2 the ALICE SDD system will be described, including the detector design and an overview of the readout architecture. In Section 3 beam test results for the spatial resolution of a final detector prototype will be discussed.

## 2. The Silicon Drift Detector system

The SDDs have to provide a spatial precision of about 30 μm, and a two-track separation down to $O(600)$ μm. In addition the charge resolution should allow a $dE/dx$ resolution dominated by Landau fluctuations.

### 2.1. The detector

The ALICE SDD final prototypes [5] were produced by Canberra Semiconductor on 300 μm thick 5″ Neutron Transmutation Doped (NTD) wafers with a resistivity of 3 kΩ cm (Fig. 1). This material was chosen because small doping fluctuations are expected from the NTD technique. The detector active area is $7.02 \times 7.53$ $cm^2$ and the ratio to the total detector area ($7.25 \times 8.76$ $cm^2$) is 0.85. The active area is split into two adjacent 35 mm long drift regions, each equipped with 256 collecting anodes (294 μm pitch) and with integrated voltage dividers for the drift and the guard regions. A careful design of the cathode strips prevents any punch-through which would deteriorate the voltage divider linearity. Since the drift velocity is very sensitive to the detector temperature ($v \propto T^{-2.4}$), the monitoring of this quantity is performed by means of three rows of 33 implanted point-like MOS charge injectors [6–8].

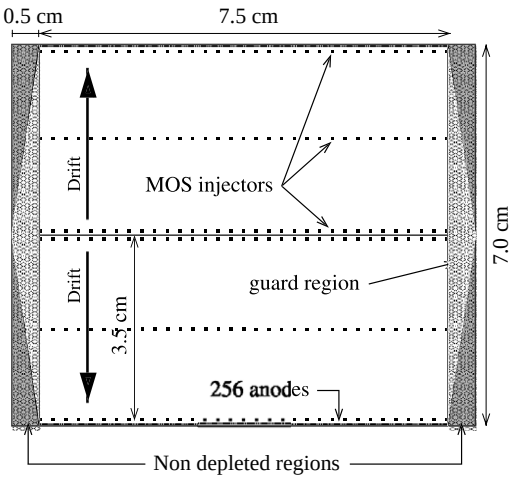


Fig. 1. Sketch of the final ALICE SDD prototype.

### 2.2. The SDD barrel

The SDDs are mounted on linear supports, called ladders, manufactured using Carbon-Fibre Reinforced Plastic (CFRP) to provide very good stiffness with minimum material budget: an SDD ladder weights 12 g and features a sag of 70 μm under a central load of 250 g. The inner SDD layer is composed of 14 ladders, each holding six detectors. It has on average a radius of 14.9 cm and a 595 mm length. The outer layer is made of 22 ladders supporting eight detectors each. It has a radius of 23.8 cm and a 670 mm length. 260 SDDs are needed to cover the two layers. In every ladder the detectors are mounted at different distances from the support structure and the ladders are assembled at different radii from the beam axis in order to allow small overlaps of the detector active areas. This is necessary to ensure the full coverage for all possible vertex positions and all tracks within the acceptance. The SDD ladders are assembled onto a CFRP mechanical support made up of two end-cap cones connected by a thin cylinder. The orientation of the SDDs anodes along the ladders, chosen to make the assembly procedure simpler, makes the drift velocity orthogonal to the beam axis and therefore to the magnetic field. The Lorenz force acts perpendicularly to the detector plane and is compensated by the focusing electric drift field.

### 2.3. SDD readout

The readout and data transmission of the whole SDD barrel is subdivided into half ladders. The total readout time of the SDD should be lower than 1 ms. A block diagram of the readout of a half ladder of the third layer is shown in Fig. 2. A 256 channel front-end hybrid circuit, connected to each half detector, performs the preamplification and the analogue to digital conversion of the SDD signal, and transmits the data to the end ladder. The power consumption of the front-end electronics has to be as low as possible due to the high sensitivity of the detector to temperature variations and to the limited material for cooling that can be located on the ladder structure. The SDD front-end electronics is based on two 64 channel

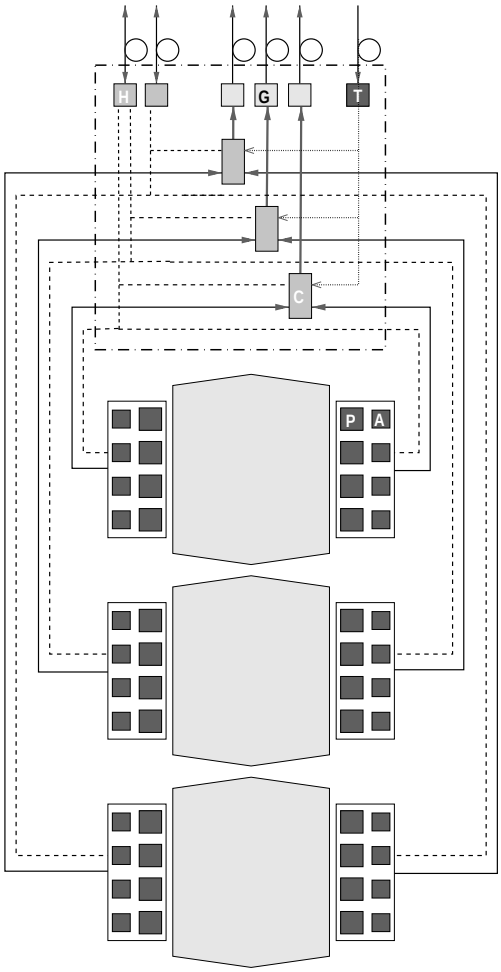


Fig. 2. Readout block diagram of a half ladder of the third layer. P: PASCAL (Preamplifier, Analogue Storage and Conversion from Analogue to digitaL); A: AMBRA (A Multievent Buffer Readout Architecture); C: CARLOS (Compression And Run Length encOding Subsystem); T: TTCrx (Timing, Trigger and Control receiver) [13]; G: GOL (Gigabit Optical Link) [12]; H: HAL (Hardware Abstraction Layer).

ASICs named PASCAL [9] and AMBRA [10]. Four pairs of chips per hybrid are needed in order to read out a half SDD.

PASCAL provides both the preamplification and the digitization. It has a dynamic range of 32 fC which is necessary to meet the requirements for low momentum particle identification. To achieve the expected spatial resolution of the detector, the preamplifier has been designed to

have an equivalent noise charge of 250 $e^-$ and the $A/D$ converter to have 10-bit precision. The clock frequency of LHC, 40 MHz, has been chosen as the sampling frequency for the SDD signal. The preamplifier peaking time (40 ns) was chosen as short as possible so as to have a satisfactory double track resolution, within the limit of ensuring a good sampling of the signal for all drift times. Since the power consumption of an $A/D$ converter operated at 40 Msample/s would be unacceptable, PASCAL contains an intermediate, 256 channel, analogue ring memory for each channel which samples the output of the preamplifier every 25 ns. When a trigger is received the contents of the analogue memories are frozen and then read out by the ADCs (one ADC per two channels) with a conversion rate of 2 Msample/s, for a total readout time of about 250 μs.

The second ASIC, AMBRA, is a multi-event buffer which is necessary in order to reduce the needed bandwidth for the data transmission without increasing the average detector dead time. The data coming from PASCAL are written in one of the four digital buffers of AMBRA which derandomizes the events. AMBRA also implements a 10-bit to 8-bit data compression using a scheme chosen to keep the percentage quantization error almost constant and lower than 1.5%.

The data are transferred at 40 MHz from the four AMBRAs of each half-detector to the end-ladder modules. A third ASIC (CARLOS) performs the zero-suppression and the compression of the data [11] before their transmission to the DAQ system through the GOL serializers [12] and over the optical links. CARLOS also takes care of the interface with the trigger system via the TTCrx chip [13].

The three ASICs, PASCAL, AMBRA and CARLOS, are implemented in a commercial 0.25 μm CMOS technology, using radiation-tolerant layout techniques developed by the CERN RD49 collaboration [14].

### 2.4. Assembly of the SDD modules

The main building element of the SDD subsystem (module) is based on a single drift detector connected to two hybrid circuits. The front-end hybrid carries four PASCAL–AMBRA pairs to equip the 256 anodes of a half-detector. Each pair PASCAL–AMBRA is first assembled with an aluminum–Upilex microcable [15] which is then TAB bonded to the hybrid circuit layer and to the detector anodes. Finally, each hybrid circuit is glued with a thermo-conductive compound on a 100 μm thick carbon fibre *heat bridge* substrate which is then clipped to the cooling tubes mounted on the sides of the ladder frames.

The interface cards between the modules and the cables to the ITS patch panels carrying signals and power are placed in the end-ladder region. One low voltage (LV) card per hybrid provide individual power supply regulation, signal interfacing to the data reduction electronics and slow control circuitry. The signal and power connection between the LV cards and the hybrids is provided by Aluminum–Upilex low thickness microcables (20 μm Upilex + 30 μm Al). One high voltage (HV) card per SDD carries the filter capacitors and DC-blocking capacitors for the injector pulses. Development of microcables capable of carrying the high voltage (up to 2.4 kV) from the HV cards to the SDD is in progress. A first prototype has been recently produced which withstands a maximum voltage of 5 kV.

## 3. Beam test results

### 3.1. Experimental details

Due to the complexity of the PASCAL ASIC, the first full chain prototype has only recently been produced. This chain was tested on the beam in October 2001 and, though the data analysis is still ongoing, the preliminary results indicate that the signal-to-noise ratio is similar to the one obtained with the previous beam test front-end electronics. The previous SDD tests were performed with the OLA [16] preamplifier. OLA is a 32-channels, low-noise, bipolar VLSI circuit, specifically designed for SDDs. Each OLA channel features a charge-sensitive preamplifier, a semi-Gaussian shaping amplifier and a symmetrical line driver. The peaking time is 55 ns for a $\delta$-like input signal and the Equivalent Noise Charge (ENC) was

measured to be $\sim 230\, e^-$ at zero detector capacitance. The preamplifier was followed by a voltage amplifier driving a 30 m long twisted-pair cable connected to a flash-ADC system [17] which sampled the signal at 40 MHz. The ADC system had 8-bit resolution and a non-linear transfer function expanding the dynamic range to 10 bits.

Since 1997, several R&D tests have been performed using CERN-PS and SpS high momentum (approximately minimum ionizing) particle beams. The typical experimental setup was built in the following way: one or more (up to three) SDD prototypes were placed on the beam line within a microstrip telescope used to measure the impact point of the particle tracks on the SDD planes. The telescope was made of up to five pairs of single sided silicon strip detectors, alternating horizontal and vertical planes. Each plane had an area of $20 \times 19.2$ mm and a strip pitch of 50 μm. Two pairs (upstream and downstream) of 2 cm-wide crossed scintillator were used to select only the particles passing through the telescope. Since the area covered by the microstrip detectors was smaller than the SDD sensitive area, the SDDs were mounted on a mobile support whose position was remotely controlled and measured with a maximum error of 30 μm.

In spite of the use of NTD wafers, quite large systematic errors on the determination of the particle impact point position, attributed to a dopant inhomogeneity, were observed on beam test data taken in 1999. The possibility to correct for these systematic errors along the anode axis was shown in Ref. [18]. In order to study more precisely this inhomogeneity and the position correction along the two axes and over a whole drift region of the detector, a test has been performed in 2000.

### 3.2. Dopant inhomogeneity and spatial resolution

Inhomogeneity of the dopant concentration alters the uniformity of the drift field superimposing a local parasitic field on the ideally constant one in the middle plane of the detector. The component of the parasitic field parallel to the drift direction locally changes the drift velocity and so causes systematic errors in the measurement of the coordinate along the drift axis. The component of the parasitic field perpendicular to the drift direction induces deviations of the electron trajectories from the ideal linear path leading to systematic errors on the anodic coordinate.

During the beam test performed in 2000 an ALICE SDD prototype of the final design, half a detector ($7.5 \times 3.5$ cm$^2$) was exposed to the beam in order to evaluate the systematic deviations and the resolution along the two axes. The local systematic deviations can be evaluated by calculating within small areas the mean value of the residuals between the cluster centroid with respect to the impact point of the particle as measured by the microstrip telescope. Fig. 3 shows in gray scale the systematic deviations $\Delta X$ of the anodic coordinate (top) and $\Delta Y$ along the drift coordinate (middle) assuming a constant drift velocity calculated for all the active area of half an SDD. The bottom plot shows as an example the systematic deviations calculated for both axes at $X = 20$ mm as a function of the drift distance. Deviation of a few tens of μm in average and with maximum values up to 400 μm are observed and must be corrected in order to reach the spatial resolution goal of about 30 μm. The circular structures centered on the middle of the wafer, clearly observed in this plot, can be attributed to the characteristic radial dependence of the dopant concentration fluctuations. In addition to these sources of electrostatic field, vertical structures are also seen. They are produced by defective electronics channels with unstable gain and/or long shaping time. The horizontal step in the middle of the second plot is caused by a short circuit between two cathodes which locally reduce the drift field. Fig. 4 shows the resolution along the anode and the drift-time directions obtained after the correction of these systematic deviations. The slight increase, from 30 to 35 μm, of the resolution along the drift direction can be attributed to the charge diffusion, which make the size of the charge cluster wider at larger drift times reducing at the same time the signal amplitude. The resolution along the anode direction has values better than 30 μm over more than 80% of the whole drift path, with the best value of 15 μm at 15 mm from

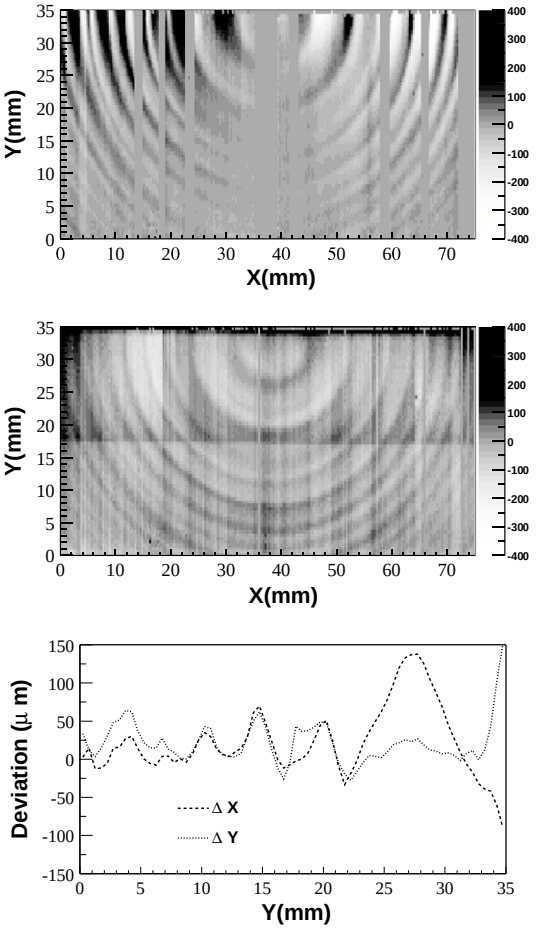


Fig. 3. Systematic deviations (gray scale in μm) of the anodic $\Delta X(X, Y)$ (top) and drift coordinates $\Delta Y(X, Y)$ (middle) of the electron cloud centroid with respect to the reference position of the crossing point of the particle coordinate, as a function of the anodic coordinate $X$, and the drift distance $Y$. Bottom plot: $\Delta X(X, Y)$ and $\Delta Y(X, Y)$ as a function of the drift distance for $X = 20$ mm.

the anodes. The deterioration of the resolution at small drift distance is due to the small size of the electron cloud collected on the anodes.

When the charge is collected by two anodes, the correction described in detail in Ref. [19] can be applied to the anode charge distribution centroid in order to better determine the position of the crossing point of the particle. The improvement due to such correction can be seen on the black circle plot of Fig. 4.

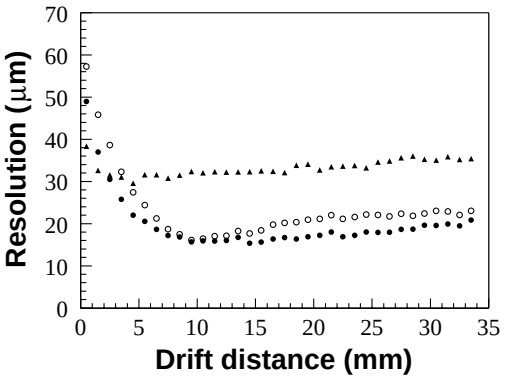


Fig. 4. Drift axis (triangles) and anode axis (white circle) spatial resolution of the ALICE SDD as function of the drift distance, after the correction of the doping inhomogeneities. Black circle: anodic resolution obtained by applying the additional two-anode cluster centroid-correction described in Ref. [19].

## 4. Conclusions

The design of the Silicon Drift Detector barrels for the ALICE Inner Tracking System is well advanced, prototypes of many critical items, like the high voltage Al-Upilex microcable, have been successfully tested. A prototype of the full front-end chain was tested on the beam in October 2001 and the preliminary results show a signal-to-noise ratio similar to the one measured with the previous OLA-based front-end electronics. The doping inhomogeneities in NTD wafers were better understood by studying the behavior of a whole half-detector using the beam test data taken in 2000. After the careful corrections of the systematic errors due to inhomogeneities, the detector spatial resolution along the drift direction was found in the range [30 : 40] μm over the whole active area with a mean value of 35 μm, and in the range [16 : 30] μm over 90% of the active area along the anode direction. These results fully satisfy the ALICE requirements. An infrared-laser mapping of the detector inhomogeneities is under study for the characterization of doping fluctuations of the 260 ALICE SDDs. The inhomogeinity pattern obtained by means of the laser is very similar to that observed in the beam test. Currently the laser mapping can account for the 80% of the

systematic errors in the position measurements observed on the beam. This preliminary result would be satisfactory for more than $\frac{3}{4}$ of the sensitive area.

## References

[1] N. Antoniou, et al., CERN/LHCC 93-16, 1993.
[2] ALICE Collaboration, CERN/LHCC 95-71.
[3] ALICE Collaboration, CERN/LHCC 99-12.
[4] F. Tosello, et al., Nucl. Instr. and Meth. A 473 (2001) 210.
[5] A. Rashevsky, et al., Nucl. Instr. and Meth. A 461 (2001) 133.
[6] V. Bonvicini, et al., Il Nuovo Cim. A 112 (1999) 137.
[7] V. Bonvicini, et al., Nucl. Instr. and Meth. A 439 (2000) 476.
[8] D. Nouais, et al., Nucl. Instr. and Meth. A 477 (2002) 99.
[9] A. Rivetti, et al., CERN/LHCC 00-41.
[10] G. Mazza, et al., CERN/LHCC 01-34.
[11] A. Werbrouck, et al., Nucl. Instr. and Meth. A 471 (2001) 281.
[12] P. Moreira, et al., http://proj-gol.web.cern.ch/proj-gol/gol_manual_1.2.pdf.
[13] J. Christiansen, et al., http://www.cern.ch/TTC/TTCrx_manual3.5.pdf.
[14] M. Campbell, et al., Nucl. Instr. and Meth. A 473 (2001) 140.
[15] A.P. De Haas, et al., CERN/LHCC 99-33.
[16] W. Dabrowski, et al., Nucl. Phys. B 44 (1995) 637.
[17] F. Balestra, et al., Nucl. Instr. and Meth. A 323 (1992) 523.
[18] D. Nouais, et al., Nucl. Instr. and Meth. A 461 (2001) 222.
[19] E. Crescio, et al., CERN/ALICE/PUB 00-29, ALICE/INT 01-09.